In beam performances of the MIMOSIS-2.1 CMOS Monolithic Active Pixel Sensor

To cite this article: Michael Deveaux *et al* 2025 *JINST* **20** C07056

View the article online for updates and enhancements.

11ᵀᴴ International Workshop
on Semiconductor Pixel Detectors for Particles and Imaging
Strasbourg, France
18–22 November 2024

In beam performances of the MIMOSIS-2.1 CMOS Monolithic Active Pixel Sensor

Michael Deveaux ⑩,[a,b,*] **Ali-Murteza Altingun,**[c] **Julio Andary,**[a]
Benedict Arnoldi-Meadows ⑩,[a] **Jerome Baudot** ⑩,[c] **Gregory Bertolone,**[c]
Auguste Besson ⑩,[c] **Norbert Bialas,**[a] **Christopher Braun,**[a] **Roma Bugiel** ⑩,[c] **Gilles Claus** ⑩,[c]
Claude Colledani,[c] **Hasan Darwish,**[a,c] **Andrei Dorokhov,**[c] **Guy Dozière,**[c] **Ziad El Bitar** ⑩,[c]
Ingo Fröhlich,[a,b] **Mathieu Goffe** ⑩,[c] **Benedikt Gutsche,**[a] **Abdelkader Himmi** ⑩,[c]
Christine Hu-Guo ⑩,[c] **Kimmo Jaaskelainen,**[c] **Oliver Keller,**[f] **Michal Koziel,**[a]
Franz Matejcek ⑩,[a] **Jan Michel** ⑩,[a] **Frederic Morel,**[c] **Christian Müntz** ⑩,[a] **Hung Pham,**[c]
Christian Joachim Schmidt,[b] **Stefan Schreiber,**[a] **Matthieu Specht** ⑩,[c] **Joachim Stroth** ⑩,[a,b,d]
Eva-dhidho Taka,[a] **Isabelle Valin** ⑩,[c] **Roland Weirich,**[a] **Yüe Zhao**[c] and **Marc Winter**[e]

[a]*Institut für Kernphysik, Goethe-Universität Frankfurt, Max-von-Laue-Straße 1, 60438 Frankfurt, Germany*

[b]*GSI Helmholtzzentrum für Schwerionenforschung GmbH, Planckstraße 1, 64291 Darmstadt, Germany*

[c]*Université de Strasbourg, CNRS, IPHC UMR 7178, 67037 Strasbourg, France*

[d]*Helmholtz Forschungsakademie Hessen für FAIR, Max-von-Laue-Straße 12, 60438 Frankfurt, Germany*

[e]*Université Paris-Saclay, CNRS/IN2P3, IJCLab, 91405 Orsay, France*

[f]*Facility for Antiproton and Ion Research GmbH, Planckstraße 1, 64291 Darmstadt, Germany*

E-mail: m.deveaux@gsi.de

Abstract: MIMOSIS is a CMOS Monolithic Active Pixel Sensor developed to equip the Micro Vertex Detector of the Compressed Baryonic Matter (CBM) experiment at FAIR/GSI. The sensor will combine an excellent spatial precision of 5 μm with a time resolution of ~5 μs and provide a peak hit rate capability of $\sim 80\,\text{MHz/cm}^2$. To fulfill its task, MIMOSIS will have to withstand ionising radiation doses of ~ 5 MRad and fluences of $\sim 7 \times 10^{13}\,\text{n}_{\text{eq}}/\text{cm}^2$.

This paper introduces the reticle size full feature sensor prototype MIMOSIS-2.1, which was improved with respect to earlier prototypes by adding on-chip grouping circuits and by improving the analog power grid. Moreover, it features for a first time a 50 μm epitaxial layer, which is found to improve the performances of the non-irradiated device significantly. We discuss the in beam sensor performances as measured during beam tests at the CERN-SPS.

---

*Corresponding author.

Contents

1   Introduction

The MIMOSIS CMOS Monolithic Active Pixel Sensor (CPS) will equip the Micro Vertex Detector (MVD) [1] of the Compressed Baryonic Matter (CBM) experiment [2], which is being built at the FAIR facility in Darmstadt, Germany. It must combine a spatial precision of ~5 µm with a thickness of ~50 µm to reach the targeted material budget of 0.3–0.5% X_0 per detector station. Moreover, a mean rate capability of slightly below $20\,\mathrm{MHz/cm^2}$ in average and of up to $80\,\mathrm{MHz/cm^2}$ for few $10\,\mu s$ is needed. CBM foresees a yearly replacement of the most irradiated sensors, which limits the required radiation tolerance to 5 MRad and $7 \times 10^{13}\,\mathrm{n_{eq}/cm^2}$.

As introduced in [3, 4], MIMOSIS relies on an industrial 180 nm CMOS imaging process. It will feature 1024 columns of 504 pixels, the latter being $30\,\mu m \times 27\,\mu m$ wide. Each pixel integrates a complete amplifier / shaper / discriminator chain, inspired by the read-out architecture of the ALPIDE sensor equipping the ALICE-ITS2 detector [5]. If the signal charge related to a particle hit exceeds the discriminator threshold, the analogue front-end samples and holds this information. At the end of a $5\,\mu s$ long integration time (frame), the hit information is forwarded to an output memory of the pixel. The output memories of the 1008 pixels composing two neighboring columns are read out by a common priority encoder, which performs a zero-suppression. The readout-priority of the pixels in the double-columns follows a meandering pattern. Typically more than one pixel fires per impinging particle. Once a firing pixel is recognized, a specific on-chip pixel grouping circuit scans the three consecutive pixels in the sense of readout priority. The information on these four pixels are encoded into one common 16-bit word. Possible further pixels of a cluster are processed separately. The data is sent out via two layers of data concentration buffers and a central elastic buffer through up to eight 320 Mbps differential data links.

As its predecessor MIMOSIS-1 (see figure 1), MIMOSIS-2 forms a full feature prototype of MIMOSIS. It hosts 128 columns of DC-coupled pixels as used in ALPIDE, and three matrices with 384, 384 and 128 columns of AC-coupled pixels (see figure 2 for details). All pixels of a sub-matrix share their steering voltages/currents and thus, within production tolerances denoted as fixed-pattern-noise (FPN), feature a common threshold. MIMOSIS-2 hosts new features like the above mentioned pixel grouping, clock triplication as needed for improved SEE tolerance, and an improved single bit flip correction fixing the issues reported in [6]. Moreover, the analogue power net biasing the pixels was improved as ohmic losses increased the FPN in MIMOSIS-1.

MIMOSIS-2.1, the error corrected version of MIMOSIS-2, was manufactured with different epitaxial layer profiles: the partially depleted standard and the likely fully depleted p-stop layout [7, 8]
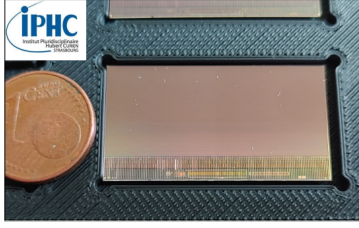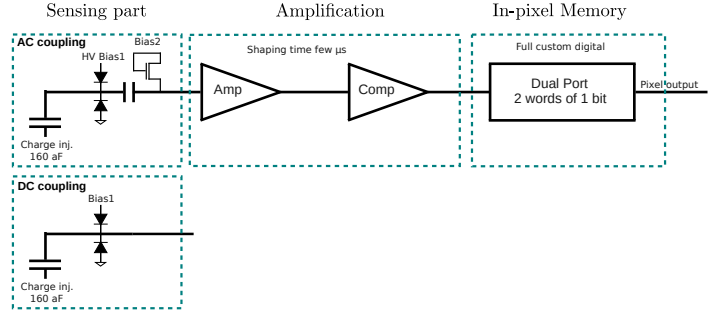
Figure 1. Photograph of the MIMOSIS-1 sensor.

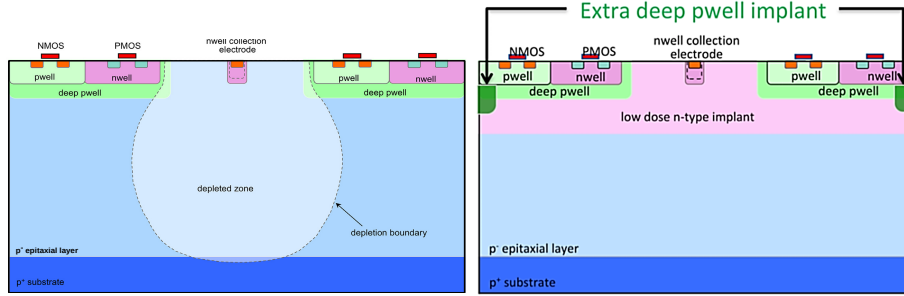**Figure 2.** Block diagram of the AC (top) and DC (bottom) coupled pixels.

Figure 3. Simplified cross-section of the standard (left) and p-stop (right) sensing node options used in MIMOSIS-2.1. Reproduced from [7]. CC BY 4.0. Reproduced from [8]. © 2020 IOP Publishing Ltd and Sissa Medialab. All rights reserved.

(see figure 3) were each combined with wafers with 25 and 50 µm thick epitaxial layer. All results shown refer to MIMOSIS-2.1, also denoted as Mi2 or MiSIS-2.1 in some captions/plots.

2 Estimate of the pixel gain

Comparing measured device performance and device simulation requires to convert measurements taken in units of mV into the number of signal electrons creating the same amplitude. The related conversion factor is found by injecting a voltage pulse ΔU to an in-pixel charge injection capacitor (see figure 2), which converts it to a signal equivalent charge according to $\Delta Q = C_{inj} \cdot \Delta U$. C_{inj} was tuned to 160 aF = 1 e/mV during the design process but it was open to which degree the design tools would provide an accurate description of such tiny capacities. As C_{inj} could initially not be measured, we had nevertheless to rely on the design value in our previous works.

The issue was addressed by measuring C_{inj} with a dedicated test structures named CE18. CE18s host either 64×32 MIMOSIS-1/2-like pixels with identical front end, collection node, injection circuit and moreover additional direct access to both, the amplifier and comparator outputs; or alternatively 64×32 SB-pixels with injection circuit and source follower as described e.g. in [9]. The latter allowed for comparing the response to $\Delta Q = 1640$ e as injected with the 5.9 keV X-rays of a ^{55}Fe-source (see [9] for details) with the one to the charge injection system. The MIMOSIS-1/2 amplifiers saturate at this ΔQ but their ToT could be calibrated and exploited in a next step.

The results based on pixels with 25 µm epitaxial layer indicate C_{inj} to deviate substantially from its design value: A C_{inj} of 1.86 e/mV and 2.02 e/mV is observed for the DC and AC pixels, respectively,

with no significant differences between standard and p-stop pixels. The individual gain of $> 90\%$ of the pixels remains within $\pm 10\%$ around the reported mean values. The new gain factors should be used to re-calibrate the electron scales of our previously published papers, namely [3, 4, 10]. Doing so will modify the communicated numerical values of quantities expressed in electrons, e.g. the sensor noise. The main performance parameters such as detection efficiency, dark rate, spatial precision, cluster multiplicity and radiation tolerance remain unchanged except that the underlying thresholds have to be interpreted in units of mV instead of units of electrons. The findings may also partially explain the correction required for matching data and simulations of the very similar ALPIDE sensor, which required a factor of 1.63 according to [11, chapter 6.4.1].

3 The MIMOSIS-2.1 beam telescope and data analysis

The detection efficiency and spatial precision of MIMOSIS-2.1 was measured in the $\sim 120\,\text{GeV}/c$ pion beam of the CERN-SPS with a MIMOSIS telescope and the TAF [12] analysis software according to the protocol previously described in [4]. Six sensor planes were placed in a distance of 1.5 cm. The outer pairs were equipped with 300 μm thick MIMOSIS-2.1 sensors with standard pixels on a 25 μm thick epitaxial layer being operated at a threshold of 120 mV. The devices under test (DUT) were installed in the two middle positions and their performance was measured as function of threshold. The threshold was set by slow control without mechanical intervention. Track alignment was performed with TAF and typically the identical alignment parameters are used for a given sensor and all thresholds while a realignment was required after exchanging the sensors. The precision was derived from the distance between the interpolated beam particle hit position and the closest hit found in the DUT within a 100 μm search window. The center-of-gravity of the hit clusters was computed to improve the spatial precision of all detector planes. Attempts to align the same data set multiple times suggest that the alignment uncertainty on the spatial precision measured remains below 0.1 μm.

Due to a failing cooling system, we operated at non-controlled room temperature (likely $T_{\text{Sensor}} \approx 30\text{–}40\,°\text{C}$). Such increased temperature may increase the leakage currents of the pixel diodes and such increase shot noise and ultimately lower the detection efficiency namely of irradiated sensors [9]. However, as the diode leakage currents of the tested, non-irradiated prototypes remain small (e.g. <1 fA per diode for MIMOSIS-1, 25 μm p-stop, 30 °C), no significant temperature effects were expected or observed.

The telescope-precision was estimated based on the software "The Telescope Optimizer" [13]. As the spatial precision of the reference planes was initially uncertain, a DUT identical to the sensors of the reference planes was used. The indicated residuals were used as precision of the reference planes. Hereafter, the indicated track precision of the telescope was folded out of the residuals of the DUT and the updated, indicated sensor precision was considered for the telescope. This approach converged after few iterations. After converging, the telescope precision obtained was fixed and used for estimating the properties of the consecutive DUTs.

4 Beam test results

The beam tests focused on AC pixels, which were hosted by 300 μm thick sensors and operated with a top bias (HV) of 10 V and a back bias of -1 V. The results are shown in figure 4. All pixels to provide a detection efficiency of $> 99.9\%$. As expected, the novel pixels with a 50 μm thick epitaxial layer (epi) outperform their 25 μm counterparts due to the increased number of signal charge carriers generated
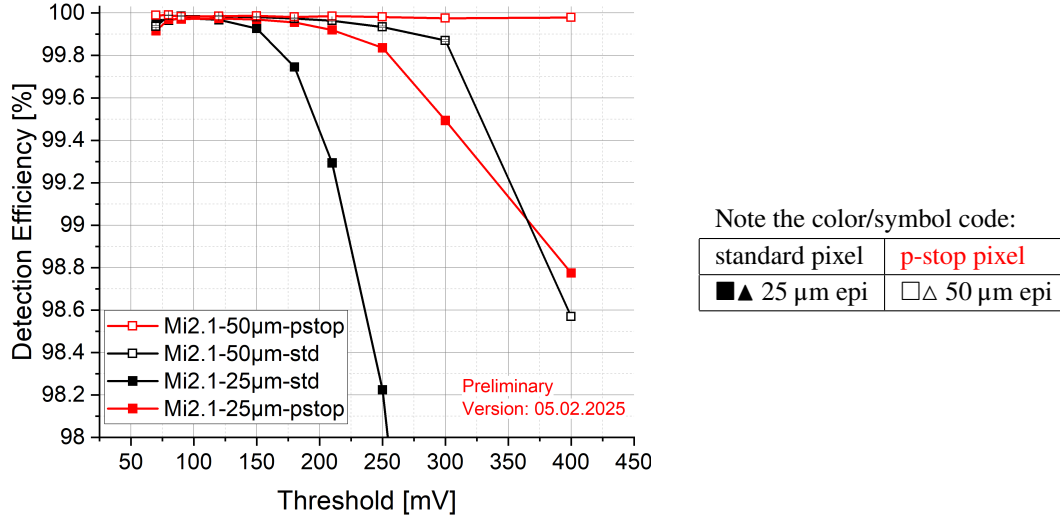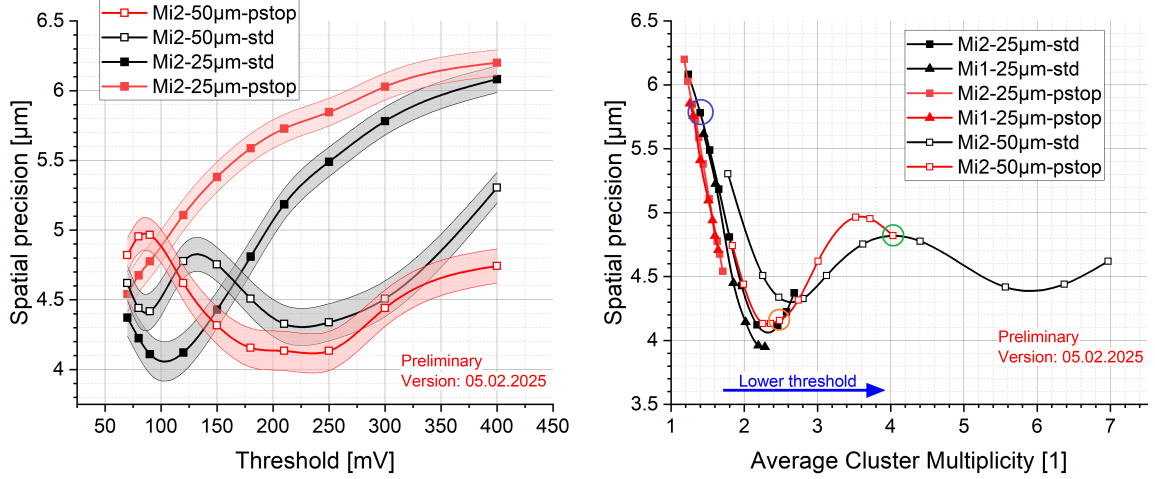
Figure 4. Detection efficiency of the pixels of MIMOSIS-2.1. Lines to guide the eye. The (statistical) uncertainties are not shown for clarity and remain below 0.02%.

in the thicker active region. Although the 25 µm pixels already achieve a >99.9% detection efficiency, leaving little room for improvement in that area, the 50 µm pixels offer a significant advantage in terms of a wider operational range and thus enhanced robustness. The observed dark rates without masking remain below the $\sim 10^{-10}$/pixel detection limit in most cases and at least one order of magnitude below the required $\sim 10^{-5}$/pixel even at lowest thresholds.
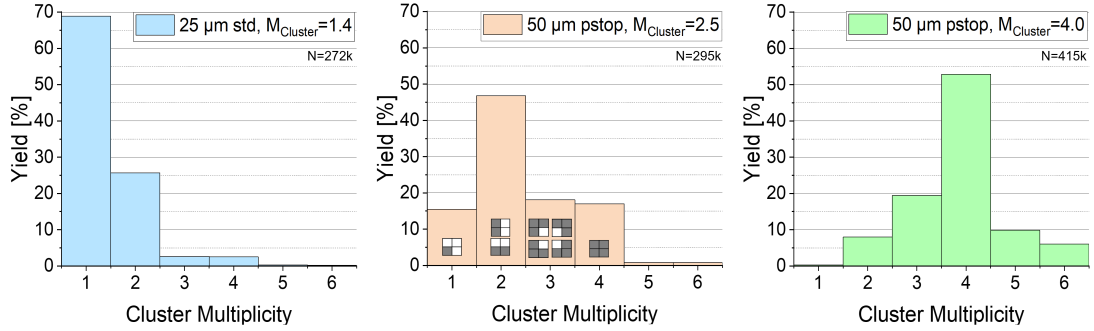
The spatial precision is displayed for the different pixel designs as function of the threshold in figure 5(a). All pixels show a precision better than 5 µm for some thresholds. Moreover, with exception of the 25 µm p-stop pixel, we observe a non-trivial dependency of this precision with increasing threshold. Once plotting the spatial precision against the cluster multiplicity (see figure 5(b)), we observe that the spatial precision seems to reach an optimum at a *mean* cluster multiplicity ($M_{cluster}$) of about 2.4, mostly independent of the pixel type. Such optimum at $M_{cluster} = 2.4$, though not mentioned by the authors of this work, is independently reported in figure 7 of [14] showing results for the pALPIDE-3b sensor equipped with a pixel similar to our 25 µm standard design.

Our current working hypothesis regarding the origin of the observed optimum is based on the use of the center-of-charge method to enhance spatial precision. Since the binary pixel output does not convey charge information, the available information is essentially limited to a small set of cluster shapes: 1×1 clusters with center-of-charge at the pixel center $\vec{x}_i$; 2×2 clusters pointing to the pixel corner located at $\vec{x}_i + (p/2, p/2)$ with p the pixel pitch; and 2×1 clusters, which point to the pixel edges at $\vec{x}_i + (0, p/2)$ or $\vec{x}_i + (p/2, 0)$, depending on orientation. Each cluster type spans its own discrete grid across the pixel matrix, with a spacing of p between grid points.[1] This results in a binary spatial resolution for each type with a known precision of $\sigma = p/\sqrt{12} = 7.8$ µm assuming $p = 27$ µm. However, because the grids are offset relative to each other, the combined effect of multiple cluster types improves the precision. If all four cluster types occur with equal frequency, they effectively form a finer grid with spacing $p/2$, leading to a theoretical precision of $\sigma = p/(2\sqrt{12}) = 3.9$ µm. Therefore, the

---

[1]This holds also for clusters with multiplicity of three (four orientations) and the numerous different, individually rare shapes with multiplicities higher than four. These clusters are neglected here for the sake of simplicity.

(a) Spatial precision vs. threshold. The error bands indicate statistical uncertainty.

(b) Spatial precision vs. cluster multiplicity. The error bars (see figure 5(a)) were removed for clarity.

(c) Cluster multiplicity for the data points encircled in figure 5(b) with according color. The cluster shapes (dark=fired) related to the multiplicity bins is sketched.

Figure 5. Spatial precision of MIMOSIS-2.1 as function of threshold (a) and M_{cluster} (b) for the short side of the $27 \times 30 \, \mu m^2$ pixel. A $\sim 10\%$ worse precision is seen for the long side (not shown). The cluster multiplicity of selected data points is histogrammed in (c). Lines to guide the eye.

highest spatial precision is expected when all four cluster types occur in equal proportions. As shown in figure 5(c), this condition is approximately fulfilled near the observed optimum at $M_{\text{cluster}} \approx 2.4$, while at lower or higher M_{cluster} values, smaller or larger clusters dominate, respectively.

5 Summary and conclusion

MIMOSIS-2.1, the first full scale full feature prototype of the future MIMOSIS CPS was tested in beam. Its four most promising pixel flavors show a detection efficiency of >99.9% in combination with negligible dark rate. The novel sensing elements relying on a $50 \, \mu m$ instead of a $25 \, \mu m$ active volume reproduce the excellent detection performances of their thinner counter parts and provide a substantially wider operational range. All pixels studied reach the targeted $5 \, \mu m$ spatial precision for suited threshold settings. We observe that best precisions are reached if the average cluster multiplicity is tuned to a value of about 2.4. It is observed that this average cluster multiplicity provides the broadest number of different clusters and such best input for the center-of-charge procedure used for improving the spatial precision of the sensor.

The absolute calibration of the threshold values in units of electrons was measured exploiting dedicated test structures. We find that the gain of the underlying charge injection system diverges by a factor of about two from its design value. A related correction factor has to be applied to quantities expressed in units of electrons (e.g. threshold and noise values) communicated in earlier publications [3, 4, 10]. The sensor performances (e.g. detection efficiency, dark rate and spatial precision) reported are not affected.

Prior to the submission of the final chip planned mid 2025, the tolerance of the 50 µm pixels to the targeted dose of 10^{14} n_{eq}/cm^2 will be evaluated. In case the 50 µm thick p-stop pixel keeps its benefits after irradiation, it might come out as the option of choice for the CBM-MVD.

Acknowledgments

References

[1] J. Stroth et al. eds., *Technical Design Report for the CBM: Micro Vertex Detector (MVD)*, GSI-2022-00549, https://fair-center.eu/user/publications/experiment-collaboration-publications#c56056.

[2] CBM collaboration, *Challenges in QCD matter physics –The scientific programme of the Compressed Baryonic Matter experiment at FAIR*, *Eur. Phys. J. A* **53** (2017) 60 [arXiv:1607.01487].

[3] M. Deveaux et al., *Observations on MIMOSIS-0, the first dedicated CPS prototype for the CBM MVD*, *Nucl. Instrum. Meth. A* **958** (2020) 162653 [arXiv:1909.05614].

[4] H. Darwish et al., *Tolerance of the MIMOSIS-1 CMOS Monolithic Active Pixel Sensor to ionizing radiation*, 2023 *JINST* **18** C06013.

[5] M. Mager, *ALPIDE, the Monolithic Active Pixel Sensor for the ALICE ITS upgrade*, *Nucl. Instrum. Meth. A* **824** (2016) 434.

[6] B. Arnoldi-Meadows et al., *Results from single event effect tests with MIMOSIS-1*, 2023 *JINST* **18** C04002.

[7] W. Snoeys et al., *A process modification for CMOS monolithic active pixel sensors for enhanced depletion, timing performance and radiation tolerance*, *Nucl. Instrum. Meth. A* **871** (2017) 90.

[8] P.M. Freeman et al., *MALTA: a Monolithic Active Pixel Sensor for tracking in ATLAS*, 2020 *JINST* **15** C03019.

[9] M. Deveaux, *Progress on the radiation tolerance of CMOS Monolithic Active Pixel Sensors*, 2019 *JINST* **14** R11001 [arXiv:1909.05715].

[10] H. Darwish et al., *Response of the MIMOSIS-1 CMOS Monolithic Active Pixel Sensor to particle beams with different dE/dx*, *Nucl. Instrum. Meth. A* **1062** (2024) 169201.

[11] M. Šuljić, *Study of Monolithic Active Pixel Sensors for the Upgrade of the ALICE Inner Tracking System*, Ph.D. Thesis, University Trieste (2018), https://hdl.handle.net/11368/2918673.

[12] IPHC-PICSEL group, *TAF analysis framework*, https://github.com/jeromebaudot/taf.

[13] M. Mager, https://mmager.web.cern.ch/telescope/tracking.html.

[14] M. Šuljić et al., *ALPIDE: the Monolithic Active Pixel Sensor for the ALICE ITS upgrade*, 2016 *JINST* **11** C11025.